Magnetic ordering in the frustrated J_1-J_2 Ising chain candidate $BaNd_2O_4$

A. A. Aczel,[1,*] L. Li,[2] V. O. Garlea,[1] J.-Q. Yan,[2,3] F. Weickert,[4] M. Jaime,[4] B. Maiorov,[4] R. Movshovich,[4] L. Civale,[4] V. Keppens,[2] and D. Mandrus[2,3,5]

[1]*Quantum Condensed Matter Division, Oak Ridge National Laboratory, Oak Ridge, Tennessee 37831, USA*
[2]*Department of Materials Science and Engineering, University of Tennessee, Knoxville, Tennessee 37996, USA*
[3]*Materials Science and Technology Division, Oak Ridge National Laboratory, Oak Ridge, Tennessee 37831, USA*
[4]*MPA-CMMS, Los Alamos National Laboratory, Los Alamos, New Mexico 87545, USA*
[5]*Department of Physics and Astronomy, University of Tennessee, Knoxville, Tennessee 37996, USA*

(Received 14 July 2014; revised manuscript received 28 August 2014; published 6 October 2014)

The AR_2O_4 family (R = rare earth) has recently been attracting interest as a new series of frustrated magnets, with the magnetic R atoms forming zigzag chains running along the c axis. We have investigated polycrystalline $BaNd_2O_4$ with a combination of magnetization, heat-capacity, and neutron powder diffraction measurements. Magnetic Bragg peaks are observed below $T_N = 1.7$ K, and they can be indexed with a propagation vector of $\vec{k} = (0,1/2,1/2)$. The signal from magnetic diffraction is well described by long-range ordering of only one of the two types of Nd zigzag chains, with collinear up-up-down-down intrachain spin configurations (double Néel state). Furthermore, low-temperature magnetization and heat-capacity measurements reveal two magnetic-field-induced spin transitions at 2.75 and 4 T for $T = 0.46$ K. The high-field phase is paramagnetic, while the intermediate-field state may arise from a spin transition of the long-range ordered Nd chains. One possible candidate for the field-induced ordered state corresponds to an up-up-down intrachain spin configuration, as predicted for a classical J_1-J_2 Ising chain with a double Néel ground state in zero field.

DOI: 10.1103/PhysRevB.90.134403 PACS number(s): 75.40.Cx, 75.30.Cr, 75.25.−j

I. INTRODUCTION

Geometric frustration is a term used to describe magnetic systems where all of the microscopic exchange interactions cannot be satisfied simultaneously, and as a consequence this class of materials often exhibits exotic magnetic ground states and complex magnetic behavior. Some common architectures characterized by frustration include pyrochlore [1], Kagome [2], and face-centered cubic magnetic sublattices [3,4]. Due to the magnetic frustration inherent in these materials, noncollinear magnetic ground states often form that can lead to multiferroic behavior [5]. In other cases, conventional long-range magnetic order is replaced by short-range alternatives, including spin glasses [6], spin liquids [7,8], and spin ices [9–11].

Recently, the family of materials AR_2O_4 (A = Ba, Sr; R = rare earth) has been attracting interest as a new series of frustrated magnets. These systems consist of two crystallographically inequivalent rare-earth sites with very different, distorted octahedral oxygen environments. Each site forms zigzag chains (or ladders) of magnetic R atoms, as illustrated in Fig. 1, running along the c axis. Bulk probes, including magnetic susceptibility and heat capacity, have shown that most members of the family have dominant antiferromagnetic (AFM) exchange interactions and relatively large frustration indices [12,13]. Geometric frustration can arise in this structure type if the next-nearest-neighbor (NNN) J_2 intrachain exchange interactions (ladder legs) are AFM and the nearest-neighbor (NN) J_1 intrachain couplings (ladder rungs) are of comparable strength.

The phase diagram for both the magnetic $S = \frac{1}{2}$ [14] and classical [15] Ising-like, AFM J_1-J_2 chain models have been determined theoretically. In both cases, a simple up-down-up-down (Néel) phase and an up-up-down-down (UUDD, double Néel) phase have been predicted depending on the relative values of J_1 and J_2. For $S = \frac{1}{2}$ systems in zero applied magnetic field, the two phases are separated by a quantum critical point at $J_2 = J_1/2$. An additional canted phase, with finite magnetization, is found between the Néel and UUDD states in the zero-field phase diagram for classical systems. In both the quantum $S = \frac{1}{2}$ and classical spin limits, the calculations predict a field-induced up-up-down (UUD) phase over a particular J_2/J_1 range for an applied magnetic field along the ordered spin direction. The UUD spin structure leads to a 1/3 magnetization plateau. Despite the extensive theoretical work on the J_1-J_2 Ising chain model, there are not many examples that can be used to test its predictions, especially in the classical limit. Some members of the AR_2O_4 family, in particular $SrDy_2O_4$ and $SrHo_2O_4$, have recently been proposed as model Ising J_1-J_2 chain systems [16]. There are also several other classical Ising chain candidates in this family with large total angular momenta J associated with the magnetic R atoms.

Several recent studies have been performed on SrR_2O_4, and both the Néel and UUDD ordering predicted by the J_1-J_2 Ising chain model have been observed in these classical magnetic spin systems. However, there are several aspects of the magnetism not explained by the original theories. For example, $SrEr_2O_4$ exhibits long-range Néel order [17], characteristic of a small J_2, coexisting with diffuse magnetic scattering [18]. Monte Carlo simulations reveal that the pattern from the latter is best described by dominant J_2 AFM exchange interactions, and this finding is consistent with quasi-one-dimensional (quasi-1D) UUDD ordering. One way the different scattering patterns can coexist is if the two types of zigzag chains have inequivalent J_1 and J_2 interactions and therefore host different

*aczelaa@ornl.gov

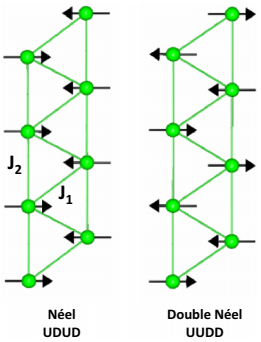

FIG. 1. (Color online) Schematics of the zigzag chain showing both the Néel and double Néel ground states that can arise from the classical J_1-J_2 Ising model, depending on the relative magnitude of the AFM J_1 and J_2 exchange interactions.

magnetic ground states. Support for this interpretation comes from Rietveld refinement of the neutron powder diffraction (NPD) data, as the best refinements arise when the long-range order is only associated with one type of Er zigzag chain [17].

A wide range of magnetic behavior is found across the SrR_2O_4 series. $SrHo_2O_4$ shows very similar magnetism to the Er analog with coexisting Néel and UUDD ordered states, although the correlation length of both states is finite [19–21]. As in the Er case, the two different structures can likely be associated with the two types of Ho zigzag chains. In contrast, NPD shows that $SrYb_2O_4$ is characterized by long-range Néel order on both Yb sites, although the ordered Yb moment is drastically suppressed on one of the two sites [22]. Finally, $SrDy_2O_4$ shows evidence for quasi-1D, UUDD magnetic correlations in zero field down to 50 mK [16], $SrTb_2O_4$ displays long-range incommensurate magnetic order arising from only one of the two Tb sites [23], and $SrTm_2O_4$ shows no signs of magnetic ordering down to 65 mK [24]. The low or nonexistent magnetic-ordering temperatures, coupled with the variety of observed behavior, suggest that some combination of competing exchange interactions, single-ion anisotropy, magnetic-dipole interactions, and low dimensionality play important roles in shaping the magnetic phase diagrams of these materials.

In this work, we expand the earlier studies of these zigzag chain systems to $BaNd_2O_4$ ($J = 9/2$) through magnetization, heat-capacity, and neutron diffraction measurements on polycrystalline samples. This material has a Curie–Weiss temperature $\theta_{CW} = -24$ K, while the measurements presented in this work indicate a magnetic transition of only $T_N = 1.7$ K. The low ordering temperature relative to θ_{CW} may be the result of magnetic frustration or low-dimensional magnetism. Neutron diffraction data show evidence for a long-range antiferromagnetic ground state that arises from only one of the two Nd sites, characterized by a propagation vector of $\vec{k} = (0,1/2,1/2)$ and the spins lying in the ab plane. Furthermore, low-temperature magnetization and heat-capacity measurements as a function of applied magnetic field reveal an intermediate field-induced ordered state and also indicate that any magnetic order is completely suppressed in an applied field of about 4 T as $T \to 0$.

II. METHODS

Single-phase polycrystalline $BaNd_2O_4$ samples were synthesized by a standard solid-state reaction method from high-purity starting materials of $BaCO_3$ and Nd_2O_3. About 15% extra $BaCO_3$ was added to compensate for the evaporation of barium. The starting materials were mixed and ground in an agate mortar and then pressed into pellets. The pellets were sintered in a flowing Ar atmosphere at 1150 °C for 8 hours. The resultant pellets were then reground and pressed into new pellets for more sintering in the Ar atmosphere at 1300 °C for 10 hours. The final product was confirmed to be single phase by laboratory x-ray powder diffraction.

Neutron powder diffraction (NPD) was performed with 5 g of polycrystalline $BaNd_2O_4$ at Oak Ridge National Laboratory using the HB-2A powder diffractometer of the High Flux Isotope Reactor. The sample was sealed in an Al sample can with He exchange gas, and a He-3 sample environment was used for the experiment with a base temperature of 300 mK. All measurements were conducted with a neutron wavelength of 2.41 Å and a collimation of 12′-open−6′. The NPD data was analyzed using the Rietveld refinement program FullProf [25] and the representational analysis software SARAh [26].

The specific heat was measured with a home-built probe based on the adiabatic heat-pulse technique in a He-3/He-4 dilution refrigerator from Oxford Instruments. The experiment was carried out in a 14 T superconducting magnet. Special care was taken to ensure the proper thermalization of the cold-pressed polycrystalline sample during the low-temperature measurements.

Magnetization measurements in fields up to 7 T were performed in a Quantum Design Magnetic Property Measurement System Superconducting Quantum Interference Device (MPMS SQUID) magnetometer. Data from 1.7 to 100 K was taken by using the standard He-4 setup. Data between 0.44 and 2 K were collected with an iQuantum He-3 insert that fits inside the MPMS sample space and utilizes the same SQUID detection system and procedure. Excellent agreement between the He-3 and He-4 data was observed in the temperature range of overlap.

III. DISCUSSION AND ANALYSIS

Magnetic susceptibility measurements of polycrystalline $BaNd_2O_4$ in an applied field $\mu_0 H = 0.1$ T are presented in Fig. 2 (plotted as $1/\chi$, i.e., $\mu_0 H/M$ vs T) and the results are in good agreement with previous work [13]. There was no observable difference for data collected under field-cooled and zero-field-cooled conditions. A broad valley is apparent in $1/\chi$ around 2.2 K, likely corresponding to the onset of an antiferromagnetic transition. The high-temperature data are well-described by a Curie–Weiss law, with the value of the Weiss temperature θ_{CW} strongly dependent on the chosen fitting range, as first discussed in Ref. [13]. Fitting the data to the Curie–Weiss law between 40 and 100 K yields $\theta_{CW} = -24$ K and an effective moment $\mu_{eff} = 3.40(1)\mu_B$. The effective moment is close to the expected value of $3.62\mu_B$ for Nd^{3+}.

Neutron diffraction data from HB-2A with a neutron wavelength of 2.41 Å are depicted in Fig. 3 at temperatures both above and below T_N. Successful Rietveld refinements

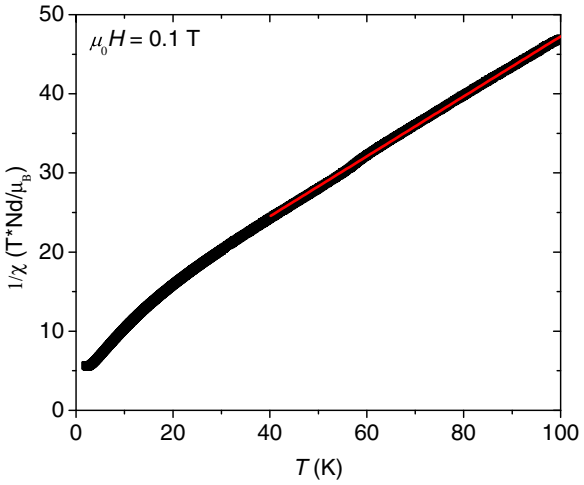

FIG. 2. (Color online) Temperature dependence of the inverse magnetic susceptibility for $BaNd_2O_4$ in an applied field of 0.1 T. The solid red line is a fit to a Curie–Weiss law in the temperature range 40–100 K. The broad valley around $T = 2.2$ K likely arises from the onset of an antiferromagnetic transition.

were performed with the known room-temperature space group *Pnam* [13,27], indicating that there are no structural phase transitions down to 300 mK. The lattice constants at 300 mK refined as $a = 10.573\,(1)$ Å, $b = 12.432\,(1)$ Å, and $c = 3.601\,(1)$ Å. Due to the excess $BaCO_3$ used in the synthesis of $BaNd_2O_4$, additional refinements were attempted where the occupancies of either the Ba or O sites were allowed to vary. No excess or deficiency of either Ba or O was found in our sample.

Several new Bragg peaks appeared below T_N, as shown in Fig. 3(b), and these could all be indexed with the propagation vector $\vec{k} = (0,1/2,1/2)$. The temperature dependence of the most intense magnetic peak $(1,1/2,1/2)$ is plotted in Fig. 3(c), with the onset clearly observed around $T_N = 1.7$ K, in good agreement with previous work [13]. Diffuse scattering nearly centered about $\vec{Q} = (1,1/2,1/2)$ is also visible and can be most clearly observed in Fig. 3(d), where neighboring resolution-limited Bragg peaks were removed from the data.

Representational analysis allowed the possible magnetic structures to be constrained on the basis of the crystal symmetry. There are two possible irreducible representations Γ_1 and Γ_2 (Kovalev's notation [28]), each with six basis vectors, and therefore there are several possible candidates for the magnetic structure of $BaNd_2O_4$. However, when refinements were attempted with several different models, the component of the Nd magnetic moments along $\hat{c}$ was consistently found to be negligible ($<0.2\mu_B$). This parameter was assumed to be zero in subsequent refinements as a result.

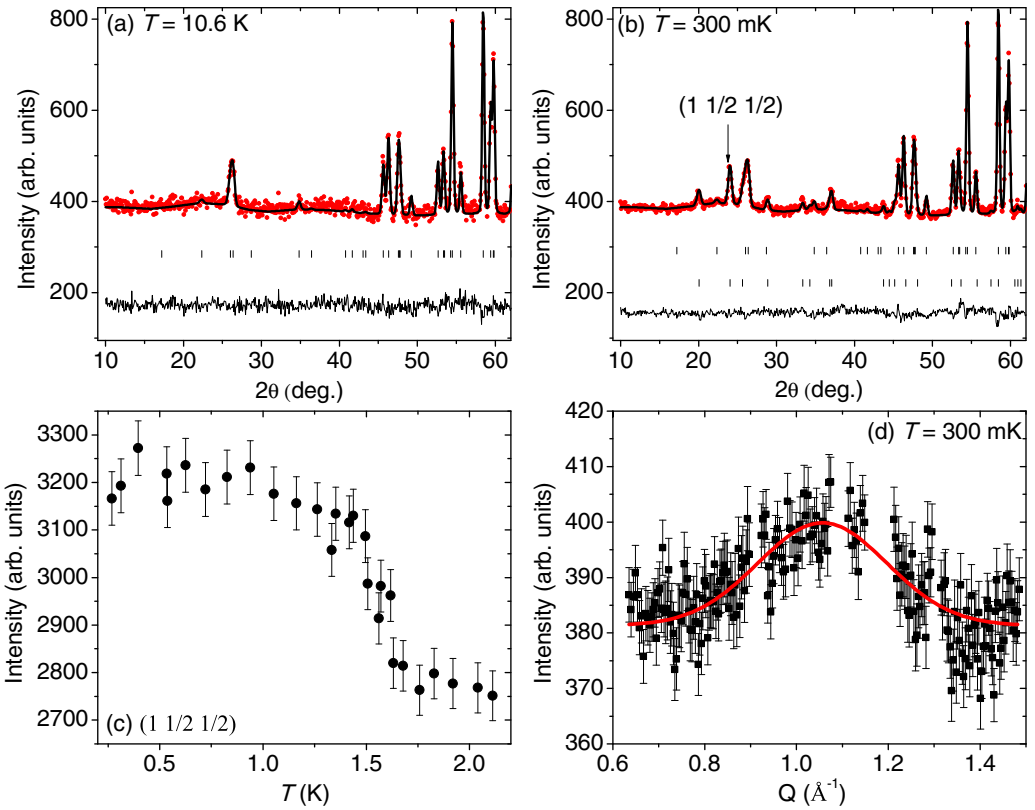

FIG. 3. (Color online) (a), (b) HB-2A neutron diffraction data with $\lambda = 2.41$ Å both above and below T_N for polycrystalline $BaNd_2O_4$. The solid lines are the fits generated from Rietveld refinements using the space group *Pnam*. One of the two most probable magnetic structures, described in the text, is also incorporated in the refinement shown at 300 mK. (c) Intensity of the $(1,1/2,1/2)$ Bragg peak plotted vs temperature. (d) A small region of the data depicted in panel (b) with the resolution-limited Bragg peaks removed, showing evidence for diffuse scattering centered around $\vec{Q} = (1,1/2,1/2)$. The solid curve is a Gaussian fit that is discussed in the text.

Recent work on the isostructural SrR_2O_4 family has emphasized the important role that the different crystal field environments of the two R sites play in governing the magnetic properties of these materials [16,21]. More specifically, neutron diffraction has generally found that the inequivalent zigzag chains host different types of magnetic order or they are characterized by different ordered moment sizes. In some cases, only one of the two R sites was found to exhibit long-range order [17]. For these reasons, refinements were attempted with equal moments on the two sites and also with the moment on one R site constrained to be zero.

The best statistical refinements correspond to the scenario where only one Nd site participates in the long-range ordering. There are four magnetic configurations that yield nearly identical fits of the data. Two of the models consist of collinear UUDD intrachain spin arrangements, which are expected for classical Ising J_1-J_2 chains in the large-AFM-J_2 limit [15]. We note that the related systems $SrHo_2O_4$ and $SrDy_2O_4$ have already been described as Ising J_1-J_2 chain systems [16]. For these reasons, the two collinear intrachain spin structures represent the most likely ordering configurations for $BaNd_2O_4$.

The other two possible models consist of noncollinear intrachain spin textures, with NNN spins along the chains AFM-coupled. These spin structures correspond to helices running along the chain direction for the special case when the NN spins are 90° out of phase (i.e., when four consecutive spins make up a complete period of the helix). While helical order is the expected ground state for an AFM Heisenberg J_1-J_2 model when $J_2 > 0.25J_1$ [15,29,30], these noncollinear models only yield equivalent statistical refinements to the UUDD models when the phases between consecutive pairs of NN spins are not constrained and refine to 63.6° and 116.4°. The resulting structures are unlikely from a physical standpoint and therefore are discarded.

The two collinear intrachain structures are presented in Figs. 4(a) and 4(b), with schematics shown for the ab plane in each case. NPD cannot determine a unique magnetic structure for $BaNd_2O_4$ because the refinements are insensitive to the rare-earth site that exhibits the long-range order, an issue first discussed for the related system $SrEr_2O_4$ [17]. The two possibilities in the present case both have Nd moments $\vec{\mu}_{Nd} = (1.39\,(1), 2.25\,(1), 0)\mu_B$. The magnitude of the moment is $2.65\,(1)\mu_B$, which is somewhat lower than the expected value of $3.3\mu_B$ for a free Nd^{3+} ion. The reduced moment may be a consequence of strong frustration, since it is impossible to satisfy all the J_1 interactions within these spin configurations whether they are AFM or FM. Figure 4(c) shows a schematic of the possible ordering patterns in the ac plane for one particular Nd zigzag chain, corresponding to the magnetic structure in Fig. 4(b). Two different domains can form with a double Néel magnetic structure, and therefore the long-range order associated with one Nd site in $BaNd_2O_4$ consists of both domain types.

The presence of the diffuse scattering below T_N is further evidence that the second Nd site is characterized by short-range correlations only. To gain additional insight into the nature of these correlations, the broad peak shown in Fig. 3(d) was fit to a simple Gaussian function. The peak center fit to $Q = 1.056\,(8)$ Å^{-1}, in good agreement with the $(1, 1/2, 1/2)$ position in reciprocal space ($Q = 1.085$ Å^{-1}). This result suggests that the short-range correlations are also characterized by a propagation vector of $(0, 1/2, 1/2)$ and therefore consistent with UUDD spin arrangements on this second type of Nd chain. The full-width half maximum (w_M) of the peak fit to $0.33\,(3)$ Å^{-1}. If one assumes that the correlation length $\zeta = 2\pi/w_M$, this corresponds to $\zeta = 19$ Å. Based on the crystal structure of this material, the short-range correlations are likely indicative of quasi-1D intrachain spin order. However, the small value of ζ makes it difficult to come to a definitive conclusion regarding the dimensionality of the short-range correlations. Although the scattering patterns for low-dimensional correlations in powders are well known (e.g., Warren lineshape for two dimensional correlations [31,32]), the defining features of these models are asymmetric lineshapes that quickly lose this asymmetry as $\zeta \to 0$ [33,34]. To better understand the origin of the diffuse scattering in $BaNd_2O_4$, it is essential to measure the correlation lengths along different directions by using a single crystal.

To further characterize $BaNd_2O_4$, the specific heat $C_p(T)$ was examined as a function of applied fields $\mu_0 H$. The λ anomaly observed in zero field is suppressed with increasing field, as shown in Fig. 5(a). Figure 5(b) depicts C_p data for $\mu_0 H > 3$ T where the anomaly at the phase transition shows significant broadening. We interpret this maximum as a Schottky peak for $\mu_0 H \geqslant 4$ T because it moves to higher temperatures with further increasing fields and it is found where our other measurements indicate that the order is suppressed. Furthermore, we estimate the entropy

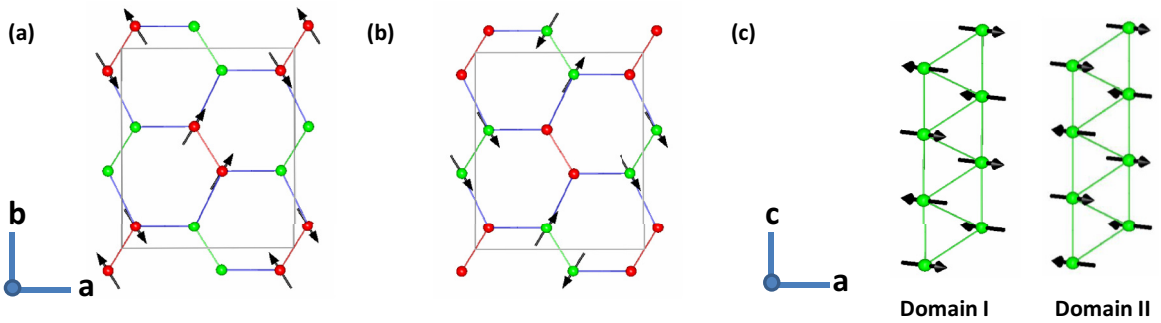

FIG. 4. (Color online) (a), (b) The two most probable magnetic structures for $BaNd_2O_4$. The two crystallographically inequivalent Nd sites are indicated by the atoms of different colors (red and green), while the two types of zigzag chains are constructed from bonds of different colors (red and green). (c) The two types of UUDD spin domains that can form along the zigzag chains.

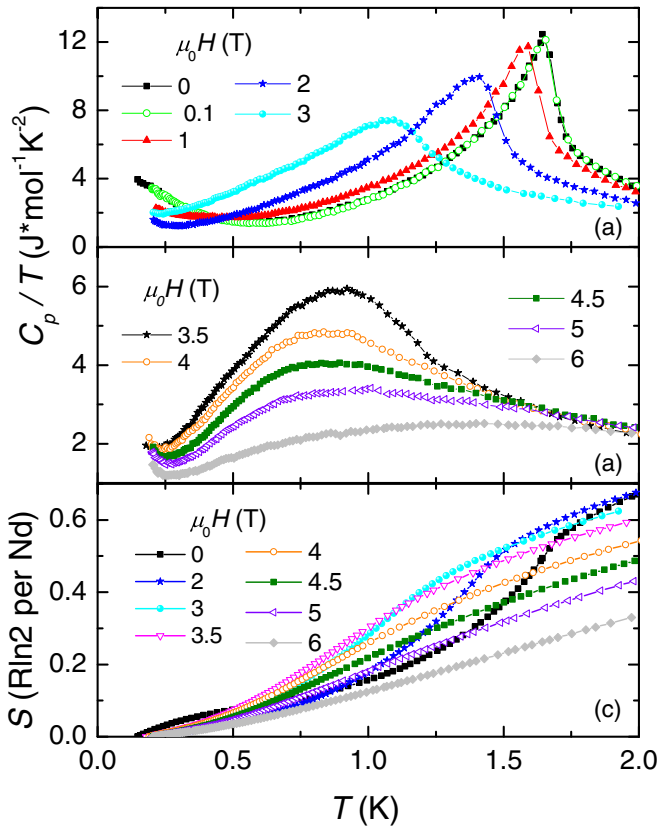

FIG. 5. (Color online) Panels (a) and (b) show specific-heat data of $BaNd_2O_4$ as C_p/T vs T in magnetic fields between 0 and 6 T. The sharp λ anomaly at 1.7 K in zero field, indicative of a magnetic phase transition, shifts down in temperature in fields up to 4 T. (c) Entropy $S(T)$ curves extracted from the C_p data for specific fields. At the phase transition, less than 5.763 J mol^{-1} K^{-1} (R ln 2) of the entropy is recovered, which supports the neutron scattering results that not every Nd atom is involved in the long-range order.

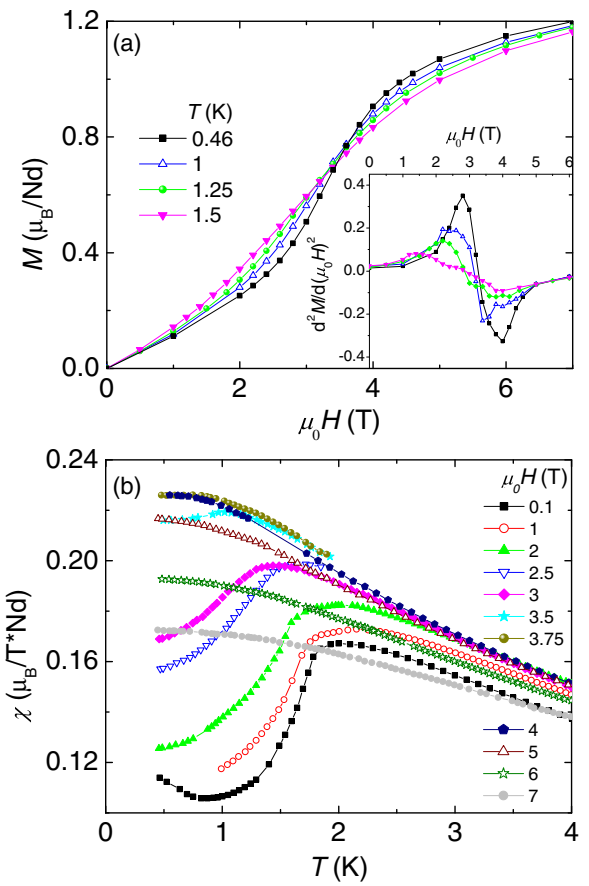

FIG. 6. (Color online) (a) Magnetization vs field data $M(\mu_0H)$ for $BaNd_2O_4$ at temperatures between 0.46 and 1.5 K. The inset shows the respective second derivatives $d^2M/d(\mu_0H)^2$. At 0.46 K, two extrema are apparent in $d^2M/d(\mu_0H)^2$ that are indicative of the two field-induced phase transitions. These features are not as clear at higher T due to thermal broadening and therefore were not used to map out the phase boundaries in this regime. (b) T dependence of the magnetic susceptibility χ for magnetic fields between 0 and 7 T. The sharp decrease in the low-field χ data with decreasing T is a signature of a phase transition from a paramagnetic to an antiferromagnetic state.

$S = \int (C_p/T)dT$ from the C_p data, with the results shown in Fig. 5(c). The jump ΔS at the phase transition in all applied fields measured is less than 5.763 J mol^{-1} K^{-1} (R ln 2) per individual Nd atom. Assuming a quasi-spin $S = \frac{1}{2}$ or even higher spin state for Nd, this small entropy gain at the transitions point to incomplete magnetic ordering among the two Nd magnetic sublattices, in good agreement with the neutron results.

Magnetization measurements $M(\mu_0H,T)$ down to 0.46 K complement the neutron scattering and C_p data. Representative M vs μ_0H measurements are shown in Fig. 6(a) with $d^2M/d(\mu_0H)^2$ vs μ_0H shown in the inset, while χ vs T is depicted in (b). The $M(\mu_0H)$ curves in (a) show an "S" shape that gets more pronounced with lower temperatures. No full saturation is observed up to 7 T. Instead, the magnetization at 7 T is only about $1.2\mu_B$ per Nd, with an extrapolated saturation value that is slightly higher ($\sim 1.3\mu_B$ per Nd), but much smaller than the expected value of $3.3\mu_B$ for a free Nd^{3+} ion. Since the two chain types seem to host different magnetic ground states, one possible explanation is that the moments are saturated by 7 T on one type of chain but not the other. This idea is supported by the neutron diffraction measurements, which found that only half the Nd moments exhibit long-range order with a Nd moment size of $2.65\mu_B$. This result corresponds to a saturation magnetization of $1.325\mu_B$ per Nd, which is in good agreement with the extrapolated value given above. A second possibility explaining the lack of full magnetization saturation is that different grains in the $BaNd_2O_4$ powder may respond to the applied field in different ways, since the Nd^{3+} ions are expected to be anisotropic.

Despite the polycrystalline nature of the sample, two extrema are observed in $d^2M/d(\mu_0H)^2$ at $\mu_0H = 2.75$ and 4 T for $T = 0.46$ K, as shown in the inset of Fig. 6(a). Similar features from magnetization data have been used previously to identify field-induced phase transitions in other magnetic systems such as $Sr_3Cr_2O_8$ [35], although these extrema in $d^2M/d(\mu_0H)^2$ only depict the transitions accurately as $T \rightarrow 0$ [36]. A similar issue seems to be apparent in the present case, as the extrema are severely broadened with increasing T.

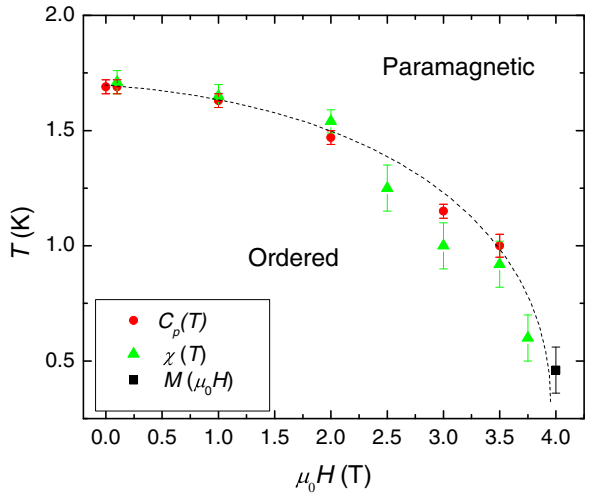

FIG. 7. (Color online) The phase diagram of polycrystalline $BaNd_2O_4$, summarizing the results from $C_p(T)$ (circles), $\chi(T)$ (triangles), and $M(\mu_0 H)$ (squares) measurements. The dashed curve serves as a guide to the eye. The long-range magnetic order with $T_N = 1.7$ K in zero field is suppressed by 4 T.

The ordering transitions are also apparent in the χ vs T data, defined by a sharp drop in χ with decreasing T. This drop is completely suppressed above 4 T, as indicated by a constant χ behavior as $T \to 0$. In low magnetic fields such as 0.1 T, a Curie–Weiss contribution to the susceptibility is observed below 0.8 K, possibly arising from a small amount of magnetic impurity or due to the Nd moments of $BaNd_2O_4$ that do not participate in the long-range magnetic ordering. However, the moments associated with this signal are fully polarized above 1 T and do not influence our experimental findings.

The most likely spin structures for the intermediate- and high-field states correspond to an UUD intrachain configuration and a paramagnetic phase, respectively. A field-induced UUD phase has been predicted for classical Ising J_1-J_2 chain systems with UUDD magnetic structures in zero field [15], as found in the present case. We note that the 1/3 magnetization plateau corresponding to the UUD state has already been found in single-crystal data of SrR_2O_4 (R = Er, Dy, Ho) [37] when $\mu_0 H$ is applied parallel to the spins within the UUDD chains. In the present case of $BaNd_2O_4$, the UUD state should give rise to a 1/3 magnetization plateau when $\mu_0 H$ is applied in the ab plane, but this feature is not expected when $\mu_0 H \parallel \hat{c}$, and therefore the plateau may get smeared out in the polycrystalline data.

The combined magnetization and heat-capacity data show that a modest magnetic field of only $\mu_0 H = 4$ T is enough to drive the system to a completely paramagnetic state, as summarized in the phase diagram presented in Fig. 7. The sharp λ anomalies observed in the C_p measurements of our polycrystalline sample, combined with the neutron scattering and magnetization results discussed above, imply that the magnetic anisotropy of $BaNd_2O_4$ is small but plays an important role in the low-temperature magnetic properties. The phase boundary between the low-field UUDD state and the intermediate-field ordered state is not indicated on the phase diagram, as this boundary is expected to be orientation dependent. The growth of $BaNd_2O_4$ single crystals would be highly beneficial for studying the T-$\mu_0 H$ phase diagrams along different crystalline directions, so the type of magnetic anisotropy and field-induced phases can be definitively established in this material.

IV. SUMMARY AND CONCLUSIONS

We have investigated polycrystalline samples of the zigzag chain system $BaNd_2O_4$ with a combination of magnetization, heat-capacity, and neutron diffraction measurements. Neutron diffraction data show evidence for resolution-limited magnetic Bragg peaks below $T_N = 1.7$ K that can be indexed with a propagation vector of $\vec{k} = (0,1/2,1/2)$. Two candidate magnetic structures are consistent with the data, each arising from long-range ordering on only one of the two types of Nd zigzag chains, with the ordered spins lying in the ab plane. The two magnetic structures are composed of UUDD spin chains, which is exactly the prediction for a classical Ising J_1-J_2 chain in the large-AFM-J_2 limit. Furthermore, low-temperature magnetization and heat-capacity measurements as a function of applied field reveal that the order can be completely suppressed in an applied field of only 4 T, with evidence found for an intermediate-field-induced state. One possibility is that the intermediate state corresponds to an UUD spin structure, also predicted for the classical Ising J_1-J_2 chain model in the large-AFM-J_2 limit. Future inelastic neutron scattering measurements and point charge calculations of the crystal field excitations for the systems in the AR_2O_4 family would help to clarify the anisotropy of the R atoms and lead to a better understanding of the magnetism in these low-dimensional frustrated magnets.

ACKNOWLEDGMENTS

The authors acknowledge useful conversations with W. Tian. This research was supported by the US Department of Energy, Office of Basic Energy Sciences. A.A.A. and V.O.G. were supported by the Scientific User Facilities Division. Work at Los Alamos, J.-Q.Y., and D.M. were supported by the Materials Science and Engineering Division. The neutron experiments were performed at the High Flux Isotope Reactor, which is sponsored by the Scientific User Facilities Division.

[1] J. S. Gardner, M. J. P. Gingras, and J. E. Greedan, Rev. Mod. Phys. **82**, 53 (2010).

[2] J. S. Helton, K. Matan, M. P. Shores, E. A. Nytko, B. M. Bartlett, Y. Yoshida, Y. Takano, A. Suslov, Y. Qiu, J. H. Chung, D. G. Nocera, and Y. S. Lee, Phys. Rev. Lett. **98**, 107204 (2007).

[3] T. Aharen, J. E. Greedan, C. A. Bridges, A. A. Aczel, J. Rodriguez, G. J. MacDougall, G. M. Luke, T. Imai,

V. K. Michaelis, S. Kroeker, H. D. Zhou, C. R. Wiebe, and L. M. D. Cranswick, Phys. Rev. B **81**, 224409 (2010).
[4] T. Aharen, J. E. Greedan, C. A. Bridges, A. A. Aczel, J. Rodriguez, G. J. MacDougall, G. M. Luke, V. K. Michaelis, S. Kroeker, C. R. Wiebe, H. D. Zhou, and L. M. D. Cranswick, Phys. Rev. B **81**, 064436 (2010).
[5] S.-W. Cheong and M. Mostovoy, Nat. Mater. **6**, 13 (2007).
[6] H. J. Silverstein, K. Fritsch, F. Flicker, A. M. Hallas, J. S. Gardner, Y. Qiu, G. Ehlers, A. T. Savici, Z. Yamani, K. A. Ross, B. D. Gaulin, M. J. P. Gingras, J. A. M. Paddison, K. Foyevtsova, R. Valenti, F. Hawthorne, C. R. Wiebe, and H. D. Zhou, Phys. Rev. B **89**, 054433 (2014).
[7] J. S. Gardner, S. R. Dunsiger, B. D. Gaulin, M. J. P. Gingras, J. E. Greedan, R. F. Kiefl, M. D. Lumsden, W. A. MacFarlane, N. P. Raju, J. E. Sonier, I. Swainson, and Z. Tun, Phys. Rev. Lett. **82**, 1012 (1999).
[8] M. J. P. Gingras, B. C. den Hertog, M. Faucher, J. S. Gardner, S. R. Dunsiger, L. J. Chang, B. D. Gaulin, N. P. Raju, and J. E. Greedan, Phys. Rev. B **62**, 6496 (2000).
[9] M. J. Harris, S. T. Bramwell, D. F. McMorrow, T. Zeiske, and K. W. Godfrey, Phys. Rev. Lett. **79**, 2554 (1997).
[10] A. P. Ramirez, A. Hayashi, R. J. Cava, R. Siddharthan, and B. S. Shastry, Nature (London) **399**, 333 (1999).
[11] B. C. den Hertog and M. J. P. Gingras, Phys. Rev. Lett. **84**, 3430 (2000).
[12] H. Karunadasa, Q. Huang, B. G. Ueland, J. W. Lynn, P. Schiffer, K. A. Regan, and R. J. Cava, Phys. Rev. B **71**, 144414 (2005).
[13] Y. Doi, W. Nakamori, and Y. Hinatsu, J. Phys.: Condens. Matter **18**, 333 (2006).
[14] J. I. Igarashi and T. Tonegawa, Phys. Rev. B **40**, 756 (1989).
[15] F. Heidrich-Meisner, I. A. Sergienko, A. E. Feiguin, and E. R. Dagotto, Phys. Rev. B **75**, 064413 (2007).
[16] A. Fennell, V. Y. Pomjakushin, A. Uldry, B. Delley, B. Prevost, A. Desilets-Benoit, A. D. Bianchi, R. I. Bewley, B. R. Hansen, T. Klimczuk, R. J. Cava, and M. Kenzelmann, Phys. Rev. B **89**, 224511 (2014).
[17] O. A. Petrenko, G. Balakrishnan, N. R. Wilson, S. de Brion, E. Suard, and L. C. Chapon, Phys. Rev. B **78**, 184410 (2008).
[18] T. J. Hayes, G. Balakrishnan, P. P. Deen, P. Manuel, L. C. Chapon, and O. A. Petrenko, Phys. Rev. B **84**, 174435 (2011).
[19] O. Young, L. C. Chapon, and O. A. Petrenko, J. Phys.: Conf. Ser. **391**, 012081 (2012).
[20] O. Young, A. R. Wildes, P. Manuel, B. Ouladdiaf, D. D. Khalyavin, G. Balakrishnan, and O. A. Petrenko, Phys. Rev. B **88**, 024411 (2013).
[21] J.-J. Wen, W. Tian, V. O. Garlea, S. M. Koohpayeh, T. M. McQueen, H.-F. Li, J.-Q. Yan, D. Vaknin, and C. L. Broholm, arXiv:1407.1341.
[22] D. L. Quintero-Castro, B. Lake, M. Reehuis, A. Niazi, H. Ryll, A. T. M. N. Islam, T. Fennell, S. A. J. Kimber, B. Klemke, J. Ollivier, V. G. Sakai, P. P. Deen, and H. Mutka, Phys. Rev. B **86**, 064203 (2012).
[23] H.-F. Li, C. Zhang, A. Senyshyn, A. Wildes, K. Schmalzl, W. Schmidt, M. Boehm, E. Ressouche, B. Hou, P. Meuffels, G. Roth, and T. Brückel, Front. Phys. **2**, 42 (2014).
[24] H.-F. Li, B. Hou, A. Wildes, A. Senyshyn, K. Schmalzl, W. Schmidt, C. Zhang, T. Brückel, and G. Roth, arXiv:1404.0044.
[25] J. Rodriguez-Carvajal, Phys. B (Amsterdam, Neth.) **192**, 55 (1993).
[26] A. S. Wills, Phys. B (Amsterdam, Neth.) **276-278**, 680 (2000).
[27] W. Wong-Ng, L. P. Cook, J. Suh, R. Coutts, J. K. Stalick, I. Levin, and Q. Huang, J. Solid State Chem. **173**, 476 (2003).
[28] O. V. Kovalev, *Representations of the Crystallographic Space Groups, Edition* 2 (Gordon and Breach Publishers, Switzerland, 1993).
[29] H. De Raedt and B. De Raedt, Phys. Rev. B **19**, 2595 (1979).
[30] I. Harada and H. J. Mikeska, Z. Phys. B: Condens. Matter **72**, 391 (1988).
[31] B. E. Warren, Phys. Rev. **59**, 693 (1941).
[32] H. Zhang, J. W. Lynn, W.-H. Li, T. W. Clinton, and D. E. Morris, Phys. Rev. B **41**, 11229 (1990).
[33] E. Granado, J. W. Lynn, R. F. Jardim, and M. S. Torikachvili, Phys. Rev. Lett. **110**, 017202 (2013).
[34] R. C. Jones, Acta Crystallogr. **2**, 252 (1949).
[35] A. A. Aczel, Y. Kohama, C. Marcenat, F. Weickert, M. Jaime, O. E. Ayala-Valenzuela, R. D. McDonald, S. D. Selesnic, H. A. Dabkowska, and G. M. Luke, Phys. Rev. Lett. **103**, 207203 (2009).
[36] A. A. Aczel, Ph.D. thesis, McMaster University, 2010.
[37] T. J. Hayes, O. Young, G. Balakrishnan, and O. A. Petrenko, J. Phys. Soc. Jpn. **81**, 024708 (2012).